Journal of Materials Chemistry C

PAPER

Reduced efficiency roll-off in light-emitting diodes enabled by quantum dot–conducting polymer nanohybrids†

Cite this: J. Mater. Chem. C, 2014, 2, 4974

Wan Ki Bae,[a] Jaehoon Lim,[b] Matthias Zorn,[c] Jeonghun Kwak,[d] Young-Shin Park,[b] Donggu Lee,[e] Seonghoon Lee,[f] Kookheon Char,*[g] Rudolf Zentel*[c] and Changhee Lee*[e]

Received 5th February 2014
Accepted 18th March 2014

DOI: 10.1039/c4tc00232f

www.rsc.org/MaterialsC

We demonstrate QLEDs implementing wider active layers (50 nm) based on QD–conducting polymer nanohybrids, which exhibit a stable operational device performance across a wide range of current densities and brightness. A comparative study reveals that the significant suppression of efficiency roll-off in the high current density regime is primarily attributed to a sufficient charge carrier distribution over the wider active layer and improved charge carrier balance within QDs enabled by the hybridization of QDs with conducting polymers. Utilization of this finding in future studies should greatly facilitate the development of high performance, stable QLEDs at high current density or luminance regime toward displays or solid-state lighting applications.

I. Introduction

Nanocrystal quantum dots (QDs) has drawn attention in light-emitting applications due to their advantageous properties, such as broad absorption but narrow emission, easy emission tunability ranging from UV to near IR, excellent photoluminescence quantum yield (PL QY) and their solution processing capability.[1] Since the first quantum dot-based light-emitting diodes (QLEDs) were demonstrated,[2] multilateral efforts have been taken to improve device performance.[3,4] Recently, QLEDs with device performances close to conventional light-emitting devices have been successfully realized (*i.e.*, peak external quantum efficiency (EQE) of 18%,[5] maximum luminance above 10 000 cd m^{-2} and an operational half-lifetime of 1000 hours at 500 cd m^{-2}).[4]

Despite rapid developments, there still remains daunting issues to be solved for their practical use. The efficiency decrease at high current densities (referred to as efficiency roll-off), particularly in the range of applicable brightness, has been considered as one of the most serious device problems, limiting their practical applications towards displays, solid-state lighting and lasers. The origin of the substantial efficiency roll-off in QLEDs, compared with conventional LEDs with a similar device structure (*i.e.*, p–i–n structure) and materials, has been suggested to be: (1) the material instability of QDs by Joule heating, (2) decrease in radiative exciton recombination rate under a high electrical field[6] and (3) exciton loss *via* non-radiative Auger recombination processes.[7,8]

While continuing progress has been made to enhance the single exciton or multicarrier recombination efficiency[9] as well as the photochemical stability of QDs,[10] the device structure remains indeed the same as a p–i–n structure with narrow and compact QD active layers (typically, 1–2 monolayers (MLs)). The reason for the limited choice in device architecture is attributed to the poor charge carrier transport properties between core–shell structured QDs stabilized with insulating organic surfactants (typically, 1 nm in length). The structural features of conventional QLEDs seem to inevitably lead to higher charge carrier (or exciton) concentrations within individual QDs, and could result in the efficiency roll-off at high current densities

[a]Photo-Electronic Hybrids Research Center, National Agenda Agenda Research Division, Korea Institute of Science and Technology, 14-gil 5, Hwarang ro, Seongbuk gu, Seoul 136-791, Korea

[b]Chemistry Division, Los Alamos National Laboratory, New Mexico 87544, USA

[c]Institute of Organic Chemistry, Johannes Gutenberg-Universität Mainz, Duesbergweg 10-14, 55099 Mainz, Germany. E-mail: zentel@uni-mainz.de; Fax: +49-6131-39-24778; Tel: +49-6131-39-20361

[d]Department of Electronic Engineering, Dong-A University, Busan 604-714, Korea

[e]Department of Electrical Engineering and Computer Science, Inter-University Semiconductor Research Center (ISRC), Seoul National University, 1 Gwanak-ro, Gwanak-gu, Seoul 151-742, Korea. E-mail: chlee7@snu.ac.kr; Fax: +82-2-877-6668; Tel: +82-2-880-9093

[f]Department of Chemistry, Seoul National University, 1 Gwanak-ro, Gwanak-gu, Seoul 151-742, Korea

[g]School of Chemical and Biological Engineering, The National Creative Research Initiative Center for Intelligent Hybrids, Seoul National University, 1 Gwanak-ro, Gwanak-gu, Seoul 151-742, Korea. E-mail: khchar@plaza.snu.ac.kr; Fax: +82-2-873-1548; Tel: +82-2-880-7431

† Electronic supplementary information (ESI) available: Synthetic procedures and optical properties for oleic acid capped QDs and poly(TPD-*b*-SSMe), UPS data for poly(TPD-*b*-SSMe), AFM images and TEM images of oleic acid capped QDs and QD–poly(TPD-*b*-SSMe) nanohybrids, and cross-sectional and plane high resolution TEM images of QD–poly(TPD-*b*-SSMe) hybrid films within devices. See DOI: 10.1039/c4tc00232f

due to the exciton loss process *via* an Auger recombination process.[7,8,11] This line of reasoning motivates our study of the correlation between the morphology of QD active layers and the performance of QLEDs.

In this study, we for the first time present a comparative study on the influence of QD morphologies to the device performances. To fully realize the morphological contrast of active materials, we prepare QD arrays with improved carrier transport properties by hybridizing QDs with conducting polymer brushes. The systematic comparison of device performance between QLEDs employing active layers with different QD morphologies (~8 MLs) reveals that the wide QD active layer leads to the reduced efficiency roll-off at high current densities compared with the narrow QD distribution (1–2 MLs) placed on top of a carrier transport layer. We attribute the reason for the reduced efficiency roll-off in QLEDs with the QD–polymer hybrids to the efficient charge distribution across the active layers and the improved charge balance within QDs. In the case of QD–conducting polymer hybrids, QDs are distributed uniformly within a hybrid matrix and therefore the exciton density across the active emissive layer is lower than for the conventional QLED structure, resulting in suppressed exciton loss even at high current densities. Moreover, the electron–hole balance within the QD–conducting polymer hybrid emissive layer can be improved due to the improved carrier injection at the interface between QDs and conducting polymer brushes. As a result, QLEDs exhibiting a stable device efficiency of 1.38% (Std. = ±0.03) over a wide range of current density (1–200 mA cm^{-2}) as well as color-saturated EL emission (FWHM = 28 nm) with the maximum brightness above 7000 cd m^{-2} have been realized. The approaches taken in the present study establish, for the first time, the detailed correlation between the reduced efficiency roll-off in QLEDs and the nanoscopic morphology of the QD active layer and thus suggest reasonable guidelines in designing materials and device architectures of QLEDs toward practical applications as full color displays and solid-state lighting.

II. Results and discussion

Various methods have been reported to improve the carrier transport properties within multilayer QD arrays either by removing the surfactants or by replacing them with short hydrocarbon chains or conductive organic/inorganic moieties.[12] Among these plausible approaches, we adopted the hybridization of QDs with conducting polymers[13,14] for the present study, not only because of the enhanced carrier transport through the conducting polymer brushes and the facilitated carrier injection–separation at the interface between QDs and conducting polymer brushes, but also due to the improved colloidal stability and the flexible processing capability of the hybrids originating from chemically grafted polymer brushes.

For QLED fabrication, QDs with a chemical composition gradient (with a diameter of 8 nm stabilized with oleic acids) are synthesized as previously reported.[10] To replace the insulating oleic acid ligand layer, a block copolymer containing a hole-conducting block was designed based on triphenylamine (TPA) units. We chose a triphenyldiamine (TPD) derivative with methoxy side groups in the *para*-position. These structures are known to be chemically and electrically stable with an improved hole carrier mobility in comparison to the standard TPA, which was used in our previous work.[13,14] The synthesized monomer was polymerized through RAFT polymerization (ESI†). This hole conducting block (55 repeating units) was used as a macrochain transfer agent to polymerize a second block. We used here a reactive ester species (pentafluorophenolacrylate) which allows the flexible introduction of variable anchor groups (30 rpu). As an anchor unit we used a protected thiol structure to prevent oxidative crosslinking. The anchor unit was synthesized by protection of cysteamine with methyl methanethiosulfonate

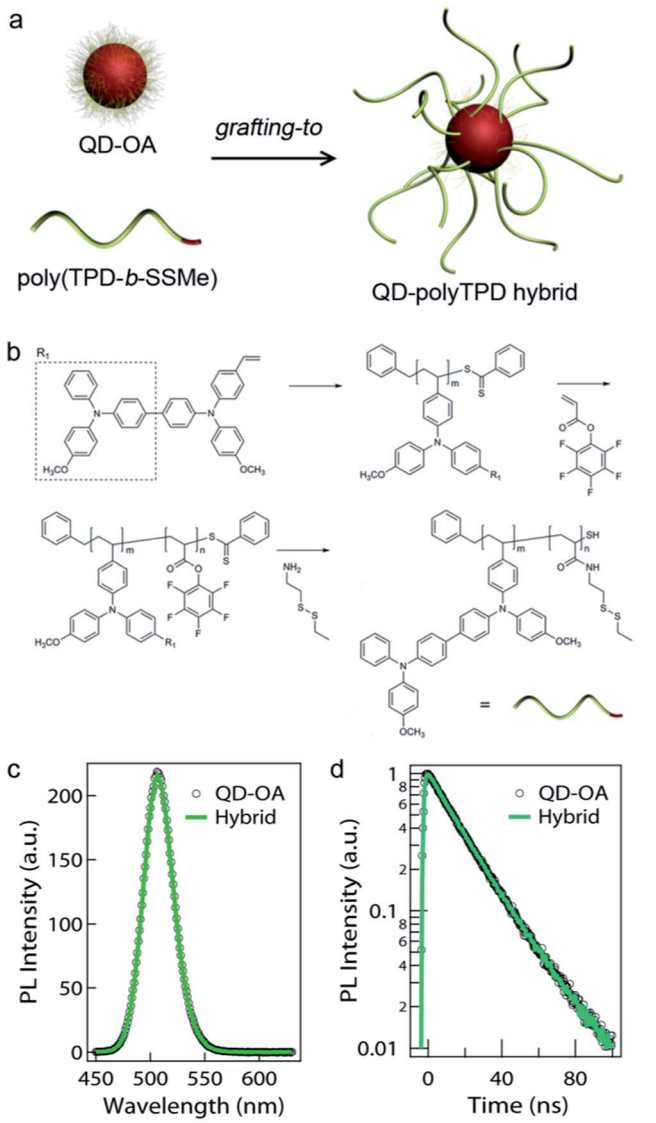

Fig. 1 (a) A schematic of the hybridization of QDs (initially stabilized with oleic acids, QD–OA) with poly(TPD-*b*-SSMe) through the *grafting-to* modification method. (b) A synthetic pathway to prepare poly(TPD-*b*-SSMe). Detailed synthetic procedures are provided in ESI.† (c) PL spectra and (d) PL decay dynamics of QDs and QD–poly(TPD-*b*-SSME) hybrids (excited at 405 nm). The single exciton dynamics within QDs are preserved throughout the surface modification process.

(MTS). The methylated disulfide (SSMe) binds efficiently to QDs but does not undergo interchain cross linking. The block copolymer (poly(TPD-*b*-SSMe)) was hybridized with the QDs through the *grafting-to* method (Fig. 1a).[13] TPD, which is widely used in OLEDs as the HTL, was chosen as the conducting moiety in this study due to its chemical and electrical stability. The HOMO and LUMO energy levels of the synthesized poly(TPD-*b*-SSMe) were determined to be as 5.6 eV and 2.6 eV, respectively, based on ultraviolet photoelectron spectroscopy (UPS) measurements and UV-visible spectra (see Fig. S3†). Even after hybridization of QDs with conducting block copolymers, the QDs maintain their initial optical properties, for example, Gaussian PL emission spectra (λ_{max} = 508 nm, FWHM = 28 nm), PL QY of 80% (excited at 420 nm) and PL decay dynamics (Fig. 1c and d), indicating that exciton decay dynamics within QD remain essentially unchanged throughout the hybridization method.

To establish the detailed correlation between QD morphology within the active layer and device characteristics, QLEDs containing the QD–poly(TPD-*b*-SSMe) hybrid film (with broad and uniform distribution of QDs within the hybrid layer) as the active layer (Device I, Fig. 2a) were designed and compared with the conventionally structured QLEDs employing the compact QD layers (1–2 MLs, with QDs in close contact with each other) placed on the charge transport layer (Device II, Fig. 2b). QDs from the same batch and organic charge transport layers with proven stability and performances were employed for both QLEDs to minimize the unexpected influence of materials to the device performances. Both devices were prepared based on a device configuration of ITO (anode)//poly(3,4-ethylenedioxythiophene):poly(styrenesulfonate) (PEDOT:PSS) (40 nm)//active layer ((QD–poly(TPD-*b*-SSMe) hybrid layer) (50 nm) (Device I) or poly(*N*,*N*′-bis(4-butylphenyl)-*N*,*N*′-bis(phenyl)benzidine) (polyTPD, 40 nm)/QD (1.5 monolayers) (Device II)//1,3,5-tris(*N*-phenylbenzimidazo l,2-yl) benzene (TPBi) (40 nm)//LiF (0.5 nm)//Al (100 nm) (cathode). PEDOT:PSS was employed to facilitate the hole injection from ITO to the active layer. TPBi was selected as the electron transporting layer (ETL) as well as the hole blocking layer. The cross-sectional TEM images in Fig. 2 clearly show the QD morphologies in QLEDs. Device I possesses the hybrid active layer (50 nm) with broad and uniform QD distribution within the conducting polymer (*i.e.*, poly(TPD-*b*-SSMe)) matrix due to energetically favorable attractions between QDs and SSMe anchor blocks. Device II possesses a compact QD emitting layer (with 1.5 QD monolayers with QDs in close contact with each other) placed between charge carrier transport layers (*i.e.*, polyTPD and TPBi). Among the devices with different QD thickness

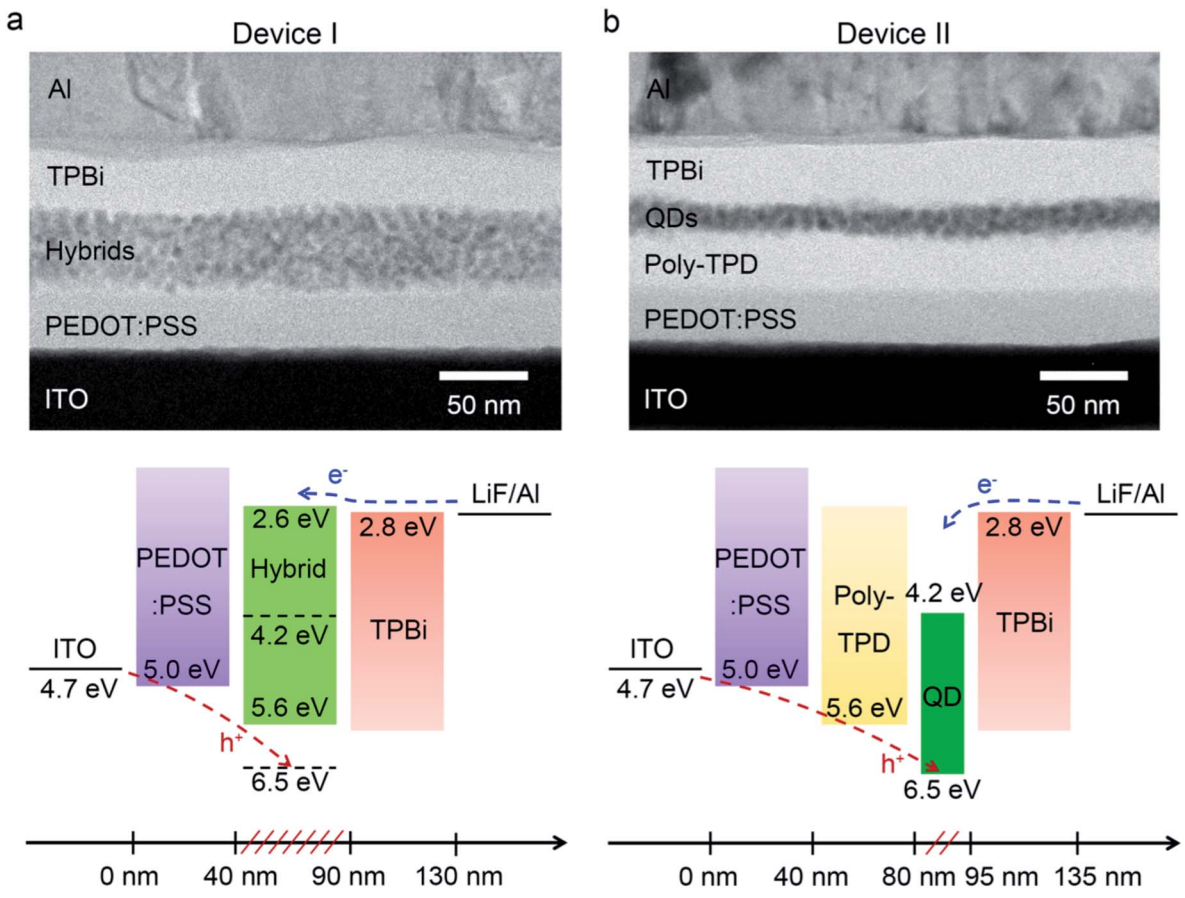

Fig. 2 Cross-sectional TEM images and energy band diagrams of (a) QLED employing a QD–poly(TPD-*b*-SSMe) hybrid layer (*ca.* ~8 MLs) as the active layer (Device I) and (b) QLED employing a pristine QD active layer (*ca.* ~1.5 MLs) placed between polyTPD and TPBi (Device II).

(*i.e.*, number of QD monolayers), the QLED (Device II) with 1.5 QD monolayers was chosen for comparison, because it exhibited the best device performance in terms of turn-on voltage, brightness, and external quantum efficiency among same device structures with different QD active layer thickness.[15] The nominal QD density within the active layers is estimated as 5.0 $\times$ 10^{12} cm^{-2} for Device I and 1.2 $\times$ 10^{12} cm^{-2} for Device II (see ESI† for discussion).

Fig. 3 shows the device characteristics (*i.e.*, current (*J*)–voltage (*V*)–luminance (*L*), EL spectrum and external quantum efficiency) of Device I and Device II. Both QLEDs exhibit narrow EL spectra with a Gaussian shape (λ_{max} = 510 nm, FWHM = 28 nm) at current densities ranging from 25 mA cm^{-2} to 150 mA cm^{-2} (Fig. 3b), which indicates that QDs are indeed the major emitting centers within the active layer for both types of QLEDs. In contrast to the previous report (in the case of the QLED with a QD monolayer sandwiched between poly-TPD), the parasitic emission from the HTL matrix was not observed in Device I, representing the efficient exciton formation within QDs enabled by the efficient carrier (electron and hole) injection from poly(TPD-*b*-SSMe) into QDs as well as the enhanced exciton transfer from poly(TPD-*b*-SSMe) to QDs. Although both devices show similar luminance profiles as a function of applied voltage, notable differences could be found in the device efficiency as a function of current density (Fig. 3c). Device I shows a stable device efficiency (Avg. EQE = 1.38%, Std.(σ) = $\pm$0.03) in current densities ranging from 1 to 200 mA cm^{-2}, while Device II shows a rather large variation in device efficiency (Avg. EQE = 1.20%, Std.(σ) = $\pm$0.11) and the drastic efficiency roll-off behavior at current densities above 50 mA cm^{-2}. We also note that the increase in the film thickness of the QD emitting layer for Device II above two QD monolayers does not improve the efficiency roll-off at higher current densities and, instead, causes a significant decrease in the current density and luminance

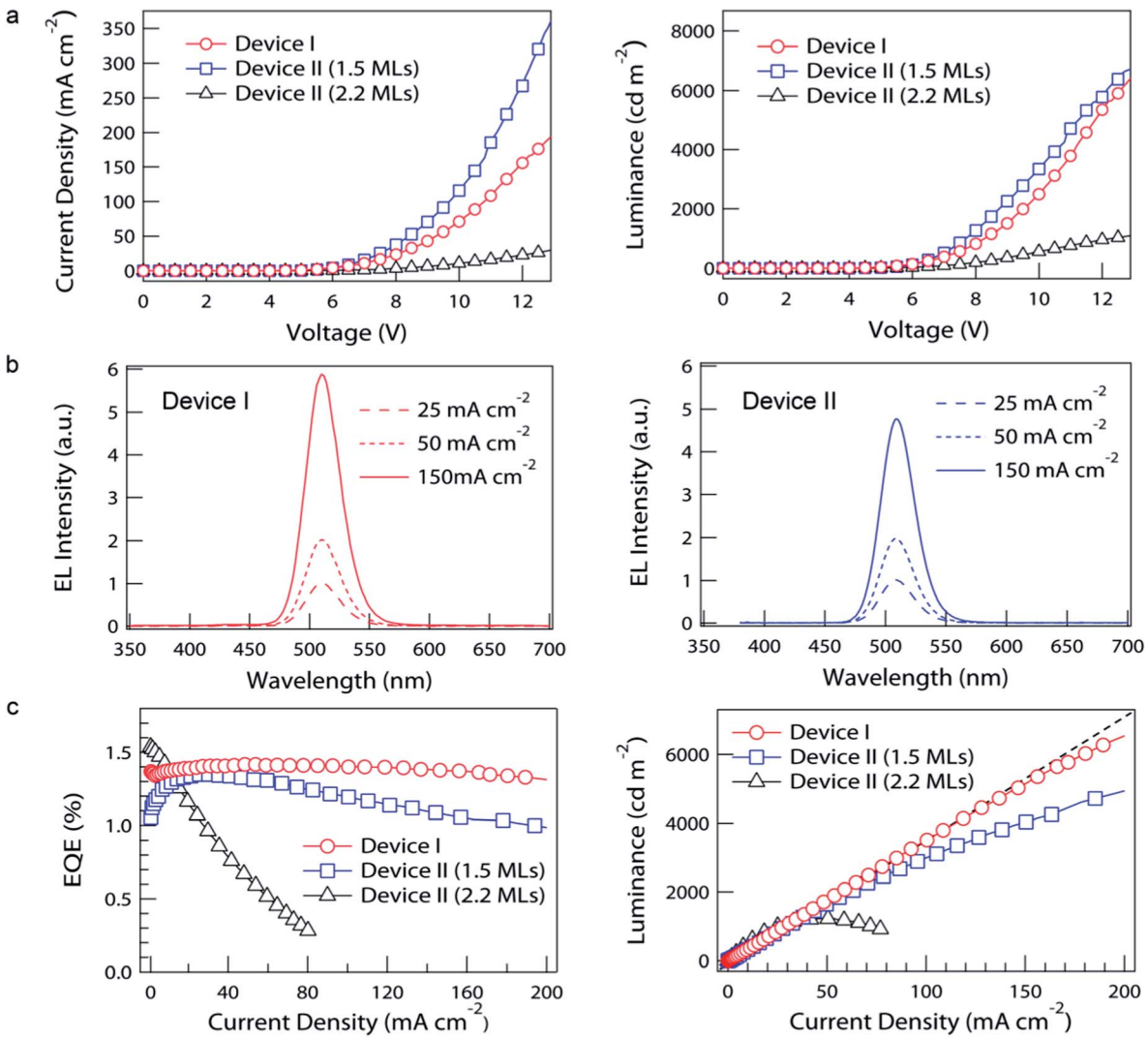

Fig. 3 (a) Current (*J*)–voltage (*V*)–luminance (*L*) characteristics, (b) EL spectra, and (c) external quantum efficiency (EQE)–current (*J*)–luminance (*L*) characteristics of QLEDs for Device I and Device II. The dotted guideline (---) in (c) (right) represents the linear increase of luminance along the current density. Note that the Device I exhibits stable device efficiency (Avg. 1.38%) over the wide current density (1–200 mA cm^{-2}), while the Device II shows the efficiency roll-off above the current density of 50 mA cm^{-2}.

as well as a pronounced efficiency roll-off as a result of insufficient charge carrier transport through the QD multilayer film.

We attribute the significant improvement in the efficiency roll-off behavior of Device I to the QD morphology within the active hybrid layer (*i.e.*, broad and uniform QD distribution within the hole transport matrix (*i.e.*, poly(TPD-*b*-SSMe)). Since QDs possess lower conduction/valence band edge energy levels (~1 eV) compared with the LUMO/HOMO energy level of typical conjugated organic molecules or polymers, the electron injection into QDs from the adjacent organic layers (*i.e.*, polyTPD or TPBi) occurs rather spontaneously (which means under little or no applied voltage) while the hole injection takes place only under the assistance of an external electric field. Moreover, the mobility of charge carriers within hole–electron transport layers (*i.e.*, polyTPD/TPBi) alters depending on the electrical field, and thus the effective exciton recombination zone shifts within the devices strongly depending on the field. In case of conventionally structured QLEDs (Device II) with a thin compact active layer consisting of one or two QD monolayers (*ca.* QD density: 1.2×10^{12} cm^{-2} in the present study), both excitons and charge carriers (particularly electrons) are accumulated within the compact QD arrays in relatively high concentration at increased current densities, leading to the exciton loss within QDs by the non-radiative Auger recombination process. By contrast, the broad QD active layer within the hole transport layer (Device I, *ca.* QD density: 5.0×10^{12} cm^{-2} in present study) enables the efficient distribution of charge carriers or excitons and also improves the charge balance within the active layer (particularly by improving the hole injection rate into QD active layers). As a consequence, the device exhibits stable efficiency even at high current densities (electrical field) due to the suppressed exciton loss.

In present study we attribute the improved efficiency roll-off of QLEDs to the broad distribution of charge carriers over QD active layers and the improved charge balance by hybridization of QDs with QD–poly(TPD-*b*-SSMe). Since Auger recombination, which universally occurs in QDs, is known to be responsible for the efficiency roll-off behavior in QLEDs,[8] we expect that our approach and results in the present study can be extended to QLEDs with better efficiency. A clear next step to further improve the device performance is the development of new conducting polymer brush layers, which can help balance charge carrier balance in QDs. The reduced hole injection barrier at the interface of the conducting polymer and QDs will enhance the charge balance within QDs and improve the device performance. We also believe that, in parallel, multilateral efforts on the synthesis of QDs with improved stability and efficiency, optimization of device structures, and better understanding of device operation or degradation mechanism will further improve the device performance, enabling the practical use of QLEDs in displays and lighting applications.

III. Summary

In summary, we presented a comparative study on the influence of morphology of QD active layers to the performance of QLEDs, particularly in terms of efficiency roll-off at high current densities and brightness. To fully realize the morphological contrast, we have prepared QD–conducting polymer hybrids (QD–poly(TPD-*b*-SSMe)) with improved charge carrier properties. In contrast to conventional QLEDs with narrow and compact QD emitting layers (*i.e.*, 1–2 MLs at most) sandwiched between HTL and ETL, QLEDs with a broad QD distribution based on the QD–poly(TPD-*b*-SSMe) hybrid active layer exhibited stable device operation (reduced efficiency roll-off) in a wide range of current densities, indicating the suppressed exciton quenching within QDs at higher current densities due to efficient distribution of excitons and carriers across the active layer as well as improved charge balance within the active layer. As a result, we could realize QLEDs with a stable device efficiency of 1.38% (Std. = ±0.03) over a wide range of current density (1–200 mA cm^{-2}) as well as the color-saturated EL emission (FWHM = 28 nm) with the maximum brightness above 7000 cd m^{-2}. The approaches and the results shown in the present study address, for the first time, the reduced efficiency roll-off in QLEDs in correlation with nanoscopic morphologies of QD active layers and thus suggest reasonable guidelines in designing materials or device architecture of QLEDs toward practical applications as full color displays and solid-state lighting.

Experimental methods

Materials

CdSe@ZnS QDs (with diameter of 8 nm) stabilized with oleic acid were synthesized as previously reported.[10] A 100 ml reaction flask containing 0.2 mmol of cadmium oxide, 4 mmol of zinc acetate and 4 ml of oleic acid was degassed under vacuum at 100 °C for 30 min, filled with nitrogen, and heated up to 300 °C. At the elevated temperature, 2 ml of trioctylphosphine dissolving 0.2 mmol of Se and 4 mmol of S was swiftly injected into the reaction flask. The reaction proceeded for 10 min and was cooled down to room temperature. QDs were purified repeatedly (5 times) and dispersed in toluene for further experiment. Poly(TPD-*b*-SSMe) was obtained by the conversion of pentafluorophenol groups in poly(TPD-*b*-PFP) with 2-(2-ethyldisulfanyl)ethanamine. A QD–poly(TPD-*b*-SSMe) hybrid solution was prepared by mixing 0.5 ml of QD dispersion (6 wt% in toluene) with 0.5 ml of poly(TPD-*b*-SSMe) solution (3 wt% in toluene). Detailed synthetic procedures are provided in the ESI.†

Device fabrication and characterization

PEDOT:PSS was first spin-cast on a patterned ITO substrate at 4000 rpm for 30 min and baked in a vacuum oven at 120 °C for 30 min. A QD–poly(TPD-*b*-SSMe) hybrid film was spin-cast at 4000 rpm for 30 s and annealed at 80 °C under N_2 atmosphere for 30 min to remove residual solvent. A polyTPD–QD bilayer film was prepared by spin-casting each solution (polyTPD in chlorobenzene (1.5 wt%) and QD in toluene (2 wt%)) consecutively at 4000 rpm for 30 s. TPBi, LiF and Al were thermally evaporated with deposition rates (monitored with a quartz-oscillator) of 1–2 Å s^{-1}, 0.1 Å s^{-1}, and 4–5 Å s^{-1}, respectively.

The current (J)–voltage (V)–luminance (L) characteristics were measured using a Keithley 236 source-measure unit and a Keithley 2000 multimeter coupled with a calibrated Si photodiode. EL spectra of the devices tested in the present study were obtained with a Konica-Minolta CS-1000A spectroradiometer.

Acknowledgements

This research was financially supported by KIST internal project (2E24821). This work was also financially supported by the National Research Foundation of Korea (NRF) funded by the Korea Ministry of Education, Science, and Technology (MEST) through the National Creative Research Initiative Center for Intelligent Hybrids (no. 2010-0018290), and Technology Development Program to Solve Climate Changes (no. NRF-2009-C1AAA001-2009-0093282). This work was also supported by the Industrial Strategic Technology Development Program (10045145, Development of high performance chalcogenide TFT backplane and cadmium-free highly efficient hybrid EL material/devices). This work was in part supported by the International Research Training Group: Self Organized Materials for Optoelectronics, jointly supported by the DFG (Germany) and NRF (Korea).

Notes and references

1 L. Brus, *J. Phys. Chem.*, 1986, **90**, 2555; A. P. Alivisatos, *Science*, 1996, **271**, 933; V. I. Klimov, *Nanocrystal Quantum Dots*, CRC, 2nd edn, 2010.

2 V. L. Colvin, M. C. Schlamp and A. P. Alivisatos, *Nature*, 1994, **370**, 354.

3 S. Coe, W.-K. Woo, M. Bawendi and V. Bulovic, *Nature*, 2002, **420**, 800; A. H. Mueller, M. A. Petruska, M. Achermann, D. J. Werder, E. A. Akhadov, D. D. Koleske, M. A. Hoffbauer and V. I. Klimov, *Nano Lett.*, 2005, **5**, 1039; J. M. Caruge, J. E. Halpert, V. Wood, V. Bulovic and M. G. Bawendi, *Nat. Photonics*, 2008, **2**, 247; L. Qian, Y. Zheng, J. Xue and P. H. Holloway, *Nat. Photonics*, 2011, **5**, 543.

4 J. Kwak, W. K. Bae, D. Lee, I. Park, J. Lim, M. Park, H. Cho, H. Woo, D. Y. Yoon, K. Char, S. Lee and C. Lee, *Nano Lett.*, 2012, **12**, 2362.

5 B. S. Mashford, M. Stevenson, Z. Popovic, C. Hamilton, Z. Zhou, C. Breen, J. Steckel, V. Bulovic, M. Bawendi, S. Coe-Sullivan and P. T. Kazlas, *Nat. Photonics*, 2013, **7**, 407.

6 Y. Shirasaki, G. J. Supran, W. A. Tisdale and V. Bulović, *Phys. Rev. Lett.*, 2013, **110**, 217403; D. Bozyigit, O. Yarema and V. Wood, *Adv. Funct. Mater.*, 2013, **23**, 3024.

7 V. I. Klimov, A. A. Mikhailovsky, D. W. McBranch, C. A. Leatherdale and M. G. Bawendi, *Science*, 2000, **287**, 1011; I. Robel, R. Gresback, U. Kortshagen, R. D. Schaller and V. I. Klimov, *Phys. Rev. Lett.*, 2009, **102**, 177404.

8 W. K. Bae, Y.-S. Park, J. Lim, D. Lee, L. A. Padilha, H. McDaniel, I. Robel, C. Lee, J. M. Pietryga and V. I. Klimov, *Nat. Commun.*, 2013, **4**, 2661, DOI: 10.1038/ncomms3661.

9 F. García-Santamaría, Y. Chen, J. Vela, R. D. Schaller, J. A. Hollingsworth and V. I. Klimov, *Nano Lett.*, 2009, **9**, 3482; F. García-Santamaría, S. Brovelli, R. Viswanatha, J. A. Hollingsworth, H. Htoon, S. A. Crooker and V. I. Klimov, *Nano Lett.*, 2011, **11**, 687; B. Mahler, P. Spinicelli, S. Buil, X. Quelin, J.-P. Hermier and B. Dubertret, *Nat. Mater.*, 2008, **7**, 659.

10 W. K. Bae, K. Char, H. Hur and S. Lee, *Chem. Mater.*, 2008, **20**, 531.

11 R. Vaxenburg, E. Lifshitz and A. L. Efros, *Appl. Phys. Lett.*, 2013, **102**, 031120; J. Iveland, L. Martinelli, J. Peretti, J. S. Speck and C. Weisbuch, *Phys. Rev. Lett.*, 2013, **110**, 177406.

12 D. V. Talapin and C. B. Murray, *Science*, 2005, **310**, 86; A. Nag, M. V. Kovalenko, J.-S. Lee, W. Liu, B. Spokoyny and D. V. Talapin, *J. Am. Chem. Soc.*, 2011, **133**, 10612; A. T. Fafarman, W.-k. Koh, B. T. Diroll, D. K. Kim, D.-K. Ko, S. J. Oh, X. Ye, V. Doan-Nguyen, M. R. Crump, D. C. Reifsnyder, C. B. Murray and C. R. Kagan, *J. Am. Chem. Soc.*, 2011, **133**, 15753.

13 M. Zorn, W. K. Bae, J. Kwak, H. Lee, C. Lee, R. Zentel and K. Char, *ACS Nano*, 2009, **3**, 1063.

14 J. Kwak, W. K. Bae, M. Zorn, H. Woo, H. Yoon, J. Lim, S. W. Kang, S. Weber, H.-J. Butt, R. Zentel, S. Lee, K. Char and C. Lee, *Adv. Mater.*, 2009, **21**, 5022.

15 W. K. Bae, J. Kwak, J. W. Park, K. Char, C. Lee and S. Lee, *Adv. Mater.*, 2009, **21**, 1690.

